JOURNAL OF MECHANICAL ENGINEERING AND SCIENCES
ISSN: 2289-4659 e-ISSN: 2231-8380
VOLUME 18, ISSUE 3, 2024, 10202 - 10222
DOI: https://doi.org/10.15282/jmes.18.3.2024.9.0806

RESEARCH ARTICLE

Extension of the displacement method by measuring reference pieces using multiple sensors for on-machine surface profile measurement

Y. Haramiishi[1], Y. A. Rahim[2], T. Shimizu[1]*, T. Ishii[1], M. F. Ali Ahmad[3], H. Watanabe[1]

[1] Faculty of Mechatronics, University of Yamanashi, Yamanashi 4008511, Japan
Phone: +81552208445, Fax.: +81552208445
[2] Faculty of Mechanical Engineering and Technology, Universiti Malaysia Perlis, Pauh Putra Campus, 02600 Arau, Perlis, Malaysia
[3] Faculty of Manufacturing and Mechatronic Engineering Technology, Universiti Malaysia Pahang Al-Sultan Abdullah, 26600 Pekan, Pahang, Malaysia

ABSTRACT - On-machine measurement is crucial in industrial production because it allows the measurement of the surface properties of products without having to remove them from the machine tool; however, measurement results are superimposed with the motion error caused by the table traverse. Therefore, eliminating motion errors is this field's main objective. This paper discusses measuring a surface profile using an extension of the displacement method to eliminate motion errors. The displacement method can separate the surface profile and motion error of the stages in measurement results; however, it introduces a specific cumulative error. The tolerance of the accumulated error was first investigated by simulating a one-axis measurement. The displacement method was extended to a two-axis stage to measure the surface profile and correct the stage tilt to each axis. Moreover, carbon steel finished using a face mill was measured in the experiments, and a coordinate measuring machine was used to compare the results with those of the extended displacement method. It was found that the extended displacement method was able to remove the motion error. Applying the displacement method resulted in an improvement of approximately 88.9%. Error analyses were also formulated and evaluated for sensor drift, reference piece measurement, motion error, table rotation, and thermal expansion, and the percentage of these errors in the total was clarified. The results showed that the motion error and table rotation for the y-axis of the prototype experimental apparatus were larger than the others. These errors are discussed to analyze each error and listed in the error budget. The proposed extended displacement method can eliminate motion errors despite the simplicity of the measurement principle and can be easily integrated into machine tools and other tables.

ARTICLE HISTORY
Received : 10th Nov. 2023
Revised : 30th Apr. 2024
Accepted : 19th Sept. 2024
Published : 30th Sept. 2024

KEYWORDS
On machine measurement
Displacement method
Surface profile
Motion error
Error compensation
Error budget

1. INTRODUCTION

On-machine measurement is an essential technique for fabrication as it can measure a workpiece profile without having to unclamp the workpiece from the machine tool. However, since machine tools always have motion errors caused by the guides and feed mechanisms, in principle, the motion errors of the machine tool are included in the on-machine measurement. Hence, separating these two components in the sensor output remains a central research issue [1, 2]. On-machine measurements, such as roundness [3, 4] and straightness measurements [5-7], have been historically employed to compensate for the motion error of the machine tool. Kono et al. [8] reduced motion errors by modeling ball screw drive systems using a Fourier series. The multi-probe method is typically used to separate motion errors from sensor outputs. Therefore, the motion error can be removed using the sequential two- and three-point methods [9, 10]. Kiyono et al. [11] developed the sequential two-point method for on-machine measurement. Hwang et al. [12] set up two probes against one probe and measured the roundness within a standard deviation of 0.05 μm. Okuyama et al. [13] also considered the two-point method with measuring errors. However, multi-probe measurement poses critical practical issues in probe size, setting, and motion errors. Another report discussed the Fourier-Eight-Sensor (F8S) method, employing eight distance sensors [14]. These sensors were processed using a Fourier series–based algorithm to separate the motion errors from straightness profiles. However, the F8S method requires eight sensors.

The displacement method that Thwaite [15] proposed can eliminate the motion error. In this procedure, reference and workpiece profiles are simultaneously measured in the first measurement, followed by a second measurement of the moved workpiece profile. This method constitutes an easy-to-use approach and a high-precision measurement technique. Thwaite proposed only the principal idea of the displacement method, and Xiaoyong et al. [16, 17] developed the displacement method to apply on-machine profile measurement for machine tools. We discuss the improvements of the displacement method applicable to built-in machine tools for planar measurement. Generally, the motion error of normal machine tools is larger than 10μm. The displacement method can separate the stage's workpiece profile and motion error. By assembling the workpiece into the machine tool, such as a machining center, measuring and machining create a precise product profile by removing the machine tool's motion error. The measurement can remove any motion error included in

*CORRESPONDING AUTHOR | T. Shimizu | ✉ tsuyoshi-s@yamanashi.ac.jp

the stage. In this respect, extending the displacement method into the traversing stage allows the motion error to be easily separated for accurate measurement. In this study, we conducted simulations and measurements for a built-in machine tool. Although linear profile measurements have been fascinating in on-machine measurement, many applications exist for measuring planar profiles. However, no progress has been made in removing the motion errors in planar profiles. This study extended the displacement method to planar measurement by considering the cumulative error and applying the simultaneous measurement method to reference pieces and the workpiece profile.

This paper discusses the principle of the displacement method, its extension to planar measurement, and the method of correcting the rotation error due to the table posture. Moreover, the measurement experiments of planar profiles were conducted to demonstrate motion error reduction using the proposed method. Finally, the errors were analyzed, and the error budget of the proposed method was discussed.

1.1 Related Work

When a product removed from a machine tool for profile measurement needs to be machined again, the product must be re-installed in the machine tool, which introduces mounting errors. On-machine measurement avoids such reinstallation errors. Therefore, on-machine measurement has been investigated for various machine tools [18-20]. Gao developed an on-machine measurement system using an atomic force microscope on a diamond-turning machine [18]. However, AFM is used in the on-machine measurement system, which provides high measurement accuracy but is unsuitable for manufacturing factories. Rhaman [19] developed an on-machine profile measurement system for an ELID grinding machine. Due to the inherently fine rotational accuracy, the measuring system specialized in grinding and removing motion errors is not considered. Kim [20] proposed fabricating free-form surfaces frequently required for constructing optical imaging systems. The system has a novel long-stroke fast tool servo on the z-axis of a diamond-turning machine. They used an on-machine measurement device to measure the optical parameters of the machined surface while compensating for the residual errors commonly produced in the diamond-turning process. The rotational accuracy of turning is high, and their measuring system is structurally accurate, so removing motion errors is not considered.

The products applied to the on-machine measurement are diverse and include lens molds and flexible beams. Zhu [21] discussed the contact and non-contact methods of on-machine measurement of aspheric lens molds. The Fringe Reflection (FR) method is introduced as a non-contact on-machine measurement method for aspherical lens molds. Whereas the leading and trailing edges represent the twisted and bent information of the blade [22], Bo [23] developed an on-machine profile measurement system consisting of a laser displacement sensor and a stylus on flexible beams to evaluate a micro-cutting-edge profile. The stylus installed on the flexible beams was in contact with the tool face, and the laser displacement sensor measured the displacement of the flexible beams. Meanwhile, many measurement principles have been developed. Pfeifer [24] proposed ultrasonic on-machine measurement based on the well-known ultrasonic time-of-flight (TOF) method in impulse/echo technique. Their method enables the evaluation of the inner topography of hollow work pieces directly on the machine. Wang [25] developed on-machine measurements of both surface shape and roughness, and their system was based on interferometry. The system enables real-time measurement and on-machine surface characterization of optical elements over various spatial frequencies and aperture sizes. Ding et al. [26] investigated the characteristics of the dependence of laser displacement transducers on the shape of the measurement object since the inclination of the measurement object affects the reflection. In addition, a novel measuring system has been proposed for the straightness error measurement of the axes of the machine tool. Borisov [27] proposed a wire mounting system with a taut wire mounted on two vertical stands along the measured axis. The optical sensors captured the lateral displacements of the head at every point of the axis traveling along the wire.

On-machine measurements have also been applied to measure the accuracy of the machine. Fan [28] proposed a six-degree-of-freedom measurement system to measure the accuracy of a linear stage. Their system can measure a moving stage's *XYZ*, roll, pitch, and yaw by detecting three parallel laser sources placed on a reference table via half mirrors. Fan [29] also developed an optical laser measurement system to measure the straightness of CMMs. Although the simple principle can separate positioning, yaw, and pitch errors, the measurement range of straightness errors is minimal because of the Doppler effect using a laser beam. However, in the case of tables with large strokes, such as machine tools, errors, such as fluctuations in the atmosphere, can quickly take over. Huan [30] proposed a toolpath compensation model based on an on-machine measurement for a 5-axis machine tool. The compensation parameter was calculated using the deviation between the nominal toolpath's measured surface and the cutter envelope surface. The machining accuracy was improved by practicing an impeller blade machining experiment. The touch trigger probe was set up on the spindle of the 5-axis machine tool, and the turbine blade was measured. As the measuring head is mounted on the spindle of the machine tool, the motion errors of the machine tool are superimposed. Jiang [31] identified 11 location errors in a five-axis machine tool's linear and rotary axes with a tilting head. They used a five-axis machine tool to machine a cubic workpiece and a laser displacement sensor to execute an on-machine measurement. The three scanning procedures were performed successively, and the measuring efficiency and accuracy of the location errors were improved. They perform error analysis with on-machine measurement using high-precision machine tools, but the motion error of the machine tool itself remains unremoved. The importance of on-machine measurements is also reaffirmed in recent studies [33-35]. Breitzke et al. [33] proposed three-dimensional artifacts to precisely measure equipment errors; raw data was collected using a 3D touch-trigger probe and used to identify geometric errors in MTs with three linear axes. Breitzke [34] used an ultra-precise 5-

axis lathe and milling machine to repeatedly clamp the machined workpiece and measure the workpiece using on-machine measurement methods. Random simulation calculations predict the theoretical error range in the repetitive positioning process. Ye et al. [35] investigate the uncertainty of on-machine surface metrology based on the chromatic confocal scanning principle. They integrate the on-machine chromatic confocal sensor into the μEDM machine tool, and they find that vibrations transmitted from neighboring machine tools enhance the driving vibrations and cause an overestimation of roughness in static noise tests. They clarified that the uncertainty due to noise is 18 nm, and the corrected flatness deviation is 50 nm. These methods are carried out with machine tools' rigidity, motion accuracy, and measuring instruments taken to the limit. However, unexpected measurement errors can easily be introduced and used on a manufacturing site, and the motion errors on the machine side can easily change. Our proposed method differs from these methods as it removes the motion errors superimposed during on-machine measurements.

2. METHODS AND MATERIALS

2.1 Displacement Method

In the displacement method, the specimen traversed a small distance in the second scanning measurement after completing the first scanning measurement for the profile acquisition. The motion error of the table can be removed by lapping both the first and second scanning results. Figure 1 shows a measurement model of this study. Sensor 1 measures the workpiece profile on the translation table, and Sensor 2 measures a profile of the reference piece that is built into the translation table. Moreover, the reference piece can be mechanically displaced. Let $w(x)$ be the profile of the workpiece, $r(x)$ be the profile of the reference piece, and $m(x)$ be the motion error of the translation table. Additionally, let the sensor output by a $SN_n(x)$, where N is the sensor number, and subscription n is the nth time measurement. Namely, sensors No. 1 and 2 output becomes $S1(x)$ and $S2(x)$, respectively, and the first scanning outputs and the second scanning outputs displacing the reference piece are represented by $S1_1(x)$ and $S1_2(x)$. Similarly, the outputs of sensor No. 2 are $S2_1(x)$ and $S2_2(x)$. Considering sensor outputs of the first scanning, $S1_1(x)$ and $S2_1(x)$ are given by the following relations:

$$S1_1(x) = w(x) + m(x) \tag{1}$$

$$S2_1(x) = r(x) + m(x) \tag{2}$$

The output from the sensor for measuring the reference piece after the reference piece is traversed $-d$ in the x-direction becomes:

$$S2_2(x) = r(x + d) + m(x) \tag{3}$$

The difference between Eq. (3) and Eq. (2) gives:

$$S2_2(x) - S2_1(x) = r(x + d) - r(x) \tag{4}$$

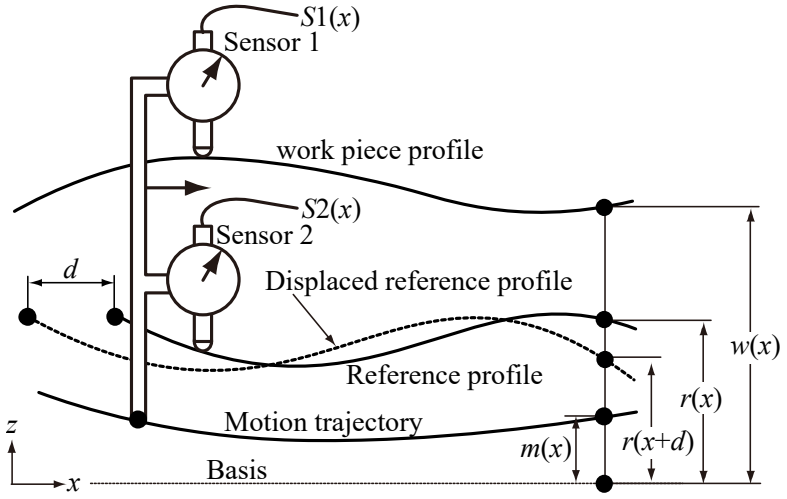

Figure 1. Geometric model of the proposed method

If d is equal to the measurement interval, Equation 4 becomes a first-order difference equation as follows:

$$S2_2(x_1) - S2_1(x_1) = r(x_1 + d) - r(x_1)\,, \tag{5}$$

$$S2_2(x_2) - S2_1(x_2) = r(x_2 + d) - r(x_2)\,, \tag{6}$$

$$S2_2(x_{k-1}) - S2_1(x_{k-1}) = r(x_{k-1} + d) - r(x_{k-1}) \tag{7}$$

where,

$$x_k = x_{k-1} + d \tag{8}$$

Therefore, the summation of Eq. (5) to Eq. (7), $r(x_k)$, yields

$$r(x_k) = \sum_{i=1}^{k-1} \{S2_2(x_i) - S2_1(x_i)\} + r(x_1) \tag{9}$$

Giving a point on $r(x_1)$ as an initial value yields $r(x)$. We obtain the motion error of the machine tool $m(x)$ from Eq. (2) after $r(x)$ is obtained. Finally, substituting $m(x)$ into Eq. (1) yields $w(x)$. As described above, by applying the displacement method to the measurement of the reference piece, $r(x)$ and $m(x)$ are calculated sequentially, and the profile of the workpiece $w(x)$ is obtained using Eq. (1).

2.2 Measurement of the Surface Profile

Applying the displacement method for an axis measurement is related to measuring the surface profile. This study extends the displacement method to two axes for surface profile measurement. Figure 2 shows the measurement model of the surface profile. Sensors No. 0, No. 1, and No. 2 are fixed to the base, and sensors No. 3 and No. 4 and the y-axis translation table are set on the x-axis translation table. Hence, sensors No. 3 and No. 4 and the y-axis translation table travel with the x-axis translation table. Moreover, a workpiece is set on the top of the y-axis translation table. Whereas sensors No. 1 and No. 2 measure the reference piece set on the x-axis translation table, sensors No. 3 and No. 4 measure the reference piece set on the y-axis translation table. Further, sensor No. 0 measures the workpiece profile.

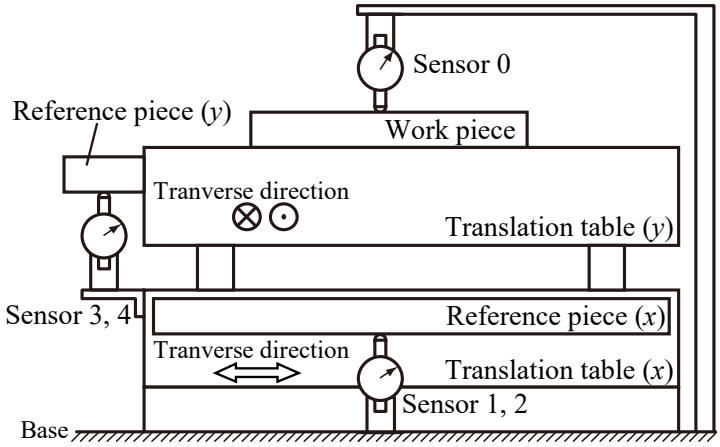

Figure 2. Measuring model for 2D surface profile

Figure 3 is the geometric model of Figure 2. $w(x, y)$ is the surface profile of the workpiece, and $r1_x(x, y)$, $r2_x(x, y)$, $r3_y(x, y)$ and $r4_y(x, y)$ are the reference piece profiles, respectively. Moreover, sensors No. 0 to 4 outputs are $Sj(x, y)(j = 0, 1, ..., 4)$. Considering motion errors, $m1_x(x, y)$ and $m2_x(x, y)$ are the motion errors of the x-axis component included in each sensor No. 1 and 2 output, respectively. Further, $m3_y(x, y)$ and $m4_y(x, y)$ are for the y-axis included in sensors No. 3 and 4 outputs. Similarly, profiles of reference pieces are $r1_x(x, y)$, $r2_x(x, y)$, $r3_y(x, y)$ and $r4_y(x, y)$ included in each output of sensor No. 1, No. 2, No. 3, and No. 4, respectively. First, when the reference piece is measured without moving from one point to another, the outputs of sensors No. 0–4 are:

$$S0_1(x, y) = w(x, y) + m_w(x, y) \tag{10}$$

$$S1_1(x, y) = r1_x(x, y) + m1_x(x, y) \tag{11}$$

$$S2_1(x, y) = r2_x(x, y) + m2_x(x, y) \tag{12}$$

$$S3_1(x, y) = r3_y(x, y) + m3_y(x, y) \tag{13}$$

$$S4_1(x, y) = r4_y(x, y) + m4_y(x, y) \tag{14}$$

In addition, because the y-axis translation table is on the x-axis translation table, $m_w(x, y)$ yields:

$$m_w(x, y) = m_{wx}(x, y) + m_{wy}(x, y) \tag{15}$$

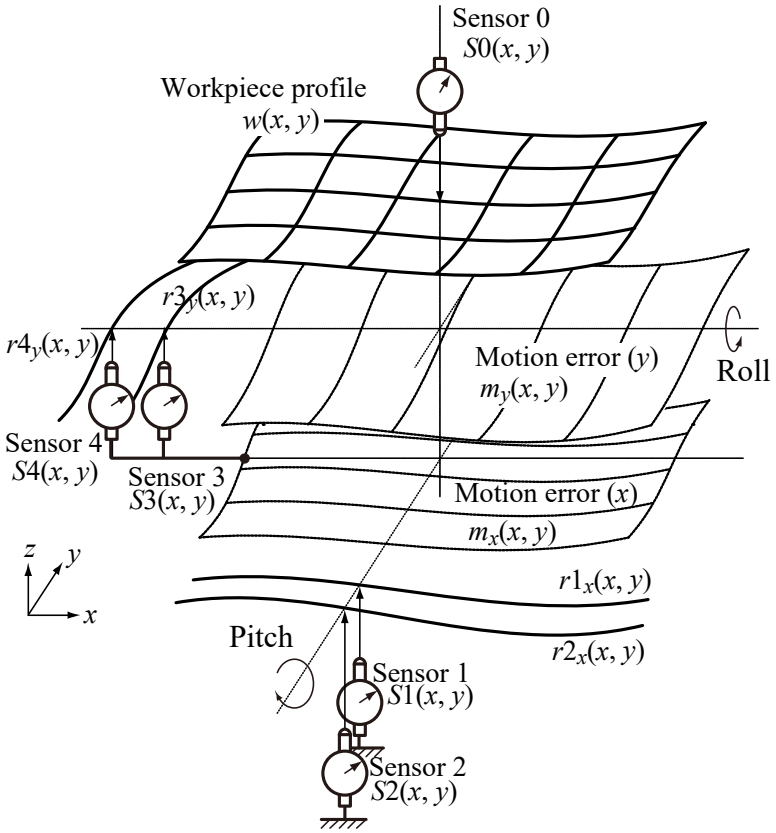

Figure 3. Geometric model of 2D profile measurement

where, m_{wx} is the motion error in the x-axis translation table, and m_{wy} is the motion error in the y-axis translation table. Next, the reference piece is traversed by a distance d in the x-axis and y-axis directions, the outputs of sensors No. 1 to 4 are:

$$S1_2(x,y) = r1_x(x+d,y) + m1_x(x,y) \tag{16}$$

$$S2_2(x,y) = r2_x(x+d,y) + m2_x(x,y) \tag{17}$$

$$S3_2(x,y) = r3_y(x,y+d) + m3_y(x,y) \tag{18}$$

$$S4_2(x,y) = r4_y(x,y+d) + m4_y(x,y) \tag{19}$$

By setting d equal to the measurement interval, the first-order difference equation is obtained using each sensor outputs $Sj_2\,(x, y)$ and $Sj_1\,(x, y)$ (j = 1, 2, 3, 4), and $r1_x\,(x, y)$, $r2_x\,(x, y)$, $r3_y\,(x, y)$ and $r4_y\,(x, y)$ are obtained. Thus, the motion errors $m1_x\,(x, y)$, $m2_x\,(x, y)$, $m3_y\,(x, y)$ and $m4_y\,(x, y)$ are calculated. If the table is traversing without rotation, the motion error of each axis is:

$$m_{wx}(x,y) = m1_x(x,y) = m2_x(x,y) \tag{20}$$

$$m_{wy}(x,y) = m3_y(x,y) = m4_y(x,y) \tag{21}$$

However, the translation table is traversing with rotation motion; rotation around the x-axis (roll), y-axis (pitch), and z-axis (yaw) will affect the sensor outputs. Nevertheless, the proposed model cannot measure the rotation around the z−axis. From this point onwards, a method for removing the effects of rotation around the x-axis (roll) and the y-axis (pitch) from the sensor outputs is discussed.

Figure 4 shows the model of the table rotation effect when measured in the x-axis direction. Sensor No. 0 measures the surface of the workpiece, and sensors No.1 and 2, which measure the reference piece, are installed along the y-axis direction. If the motion error caused by the rotation around the x-axis is zero, the outputs from sensors No. 1 and 2 will be equal. However, the outputs from sensors No. 1 and 2 are different because of the influence of the motion error components caused by the rotation around the x-axis, and the output is enlarged or reduced according to the distance between sensors No. 1 and No. 2. Therefore, the outputs of sensors No. 1 and 2 obtained during measurement in the x-axis direction include the motion error caused by rotation around the x-axis.

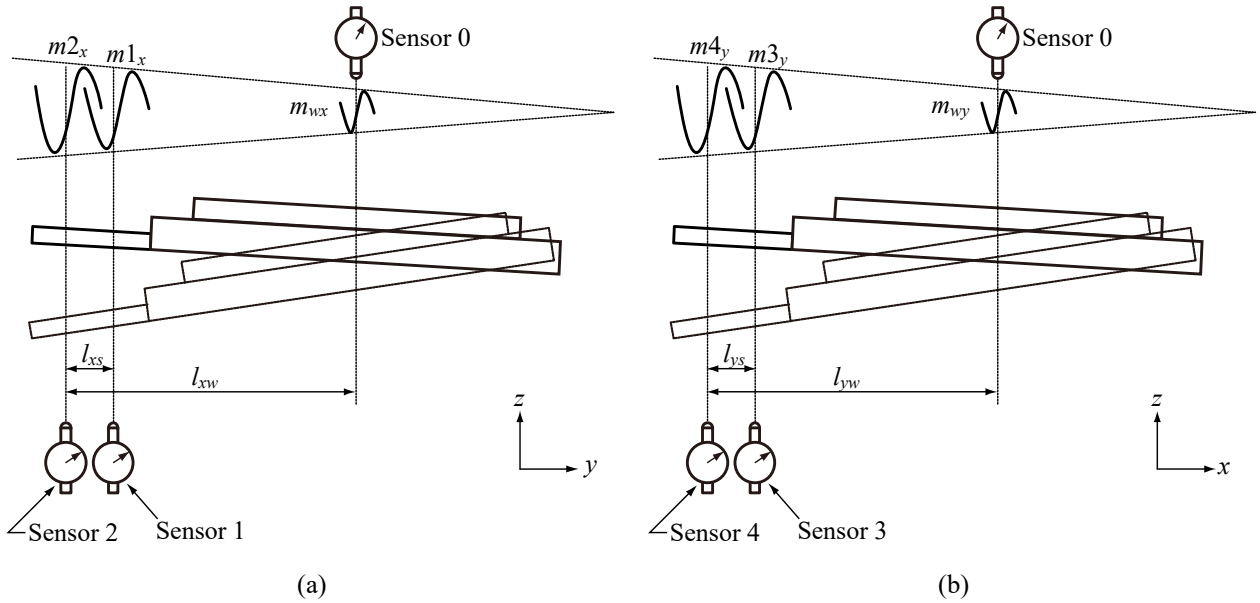

Figure 4. (a) Effect of roll around the x-axis; viewpoint from the x-axis plus to the minus direction in Figure 3 and (b) Effect of pitch around the y-axis; viewpoint from the y-axis plus to the minus direction in Figure 3

Here, the distance between sensors No. 1 and 2 is l_{xs}, and the distance between sensors No. 2 and 0 is l_{xw}. Let $m1_x\,(x, y)$ be the motion error component at the location of sensor No. 1 and let $m2_x\,(x, y)$ be the motion error component at the location of sensor No. 2. m_{wx}, $m1_x\,(x, y)$, and $m2_x\,(x, y)$ are treated similarly when the motion error just below sensor No. 0 is $m_{wx}\,(x, y)$. Let Δm_x be the difference between $m1_x\,(x, y)$ and $m2_x\,(x, y)$ as:

$$\Delta m_x = m2_x(x, y) - m1_x(x, y) \tag{22}$$

m_{wx} is obtained as:

$$m_{wx}(x, y) = m2_x(x, y) - m_{wxe}(x, y) \tag{23}$$

where, $m_{wxe}(x, y)$ is expressed as an error due to the table rotation on the x-axis,

$$m_{wxe}(x, y) = \frac{\Delta m_x(x, y)}{l_{xs}} l_{xw} \tag{24}$$

Similarly, consider the rotation around the y-axis, where a similar problem is faced. The output of sensor No. 0 is enlarged or reduced due to the distance between sensors 3 and 4. Further, sensors No. 3 and 4 outputs include the motion error caused by rotation around the y-axis during measurement. For rotation around the y-axis, the following equations are obtained.

$$m_{wy}(x, y) = m4_y(x, y) - m_{wye}(x, y) \tag{25}$$

$$m_{wye}(x, y) = \frac{\Delta m_y(x, y)}{l_{ys}} l_{yw} \tag{26}$$

where $\Delta m_y\,(x, y)$ is the difference between $m3_y\,(x, y)$ and $m4_y\,(x, y)$, and l_{ys} is the distance between sensor No. 3 and 4, and l_{yw} is the distance between sensor No. 3 and 0. Further, $m_{wye}\,(x, y)$ is expressed as an error due to the table rotation on the y-axis. Hence, $m_w\,(x, y)$ yields:

$$m_w(x, y) = m2_x(x, y) + m4_y(x, y) - m_{wxe}(x, y) - m_{wye}(x, y) \tag{27}$$

Finally, by applying Eq. (27) into Eq. (10), the workpiece $w(x, y)$ profile is obtained.

2.3 Experiments Study

2.3.1 Simulation of straight profile measurement

This section discusses applying the displacement method to the proposed method for the straight profile measurement simulation with the error. In the actual measurement, the measurement errors are included in Eq. (2) and Eq. (3). By conducting simulations under completely ideal conditions only with noise on the sensor, it is possible to know the range of sensor noise that enables profile measurement using the proposed method. In the principle of the Displacement method, d should be the same as the measurement interval, which results in a single difference equation. If a positioning error occurs in d, Eq. (8) becomes $x_k \neq x_{k-1} + d$ and therefore $r(x_{k-1} + d) - r(x_k) \neq 0$ in the difference equation and an

error occurs. Furthermore, sensor noise occurs as an error for each measurement. These errors occur for each measurement and are denoted as $\delta(x_k)$, Eq. (9) can be rewritten as:

$$r(x_k) = -\sum_{i=1}^{k-1}\{S2_2(x_i) - S2_1(x_i)\} + r(x_1) + \sum_{i=1}^{k}\delta(x_k)\,. \tag{28}$$

The accumulated error shown in the third term of Eq. (28) is simulated to determine the effect of measuring the workpiece profile. Figure 5 shows the shape of the inputs. $w(x)$, the profile of the workpiece is a square wave of 500 μm in height, and $m(x)$, the motion error of the table, is a sinusoidal wave with an amplitude of 20μm. $r(x)$, the profile of the reference piece, is a linear shape. Moreover, variations as noise added in the simulation are normally distributed with a standard deviation of 2 μm, and the measurement length is 120 mm. Figure 6 shows the shape of $r(x)$ derived from Eq. (28). The solid line indicates the shape of the reference profile $r(x)$, and the dashed line $r_c\,(x)$ indicates the calculation result of the reference profile $r(x)$. Moreover, the error is expressed as the difference between $r(x)$ and $r_c\,(x)$. The shape of the reference profile is reconstructed. In this case, the maximum error was observed to be approximately 4 μm. This error is different for each measurement, so the mean and standard deviation were examined at each position for 1000 repetitions. Figure 7 displays the simulation result of a reference profile calculation and the standard deviation of each position. The dashed line indicates the shape of the input reference profile $r(x)$, and the solid line indicates the mean of the calculation results for each position.

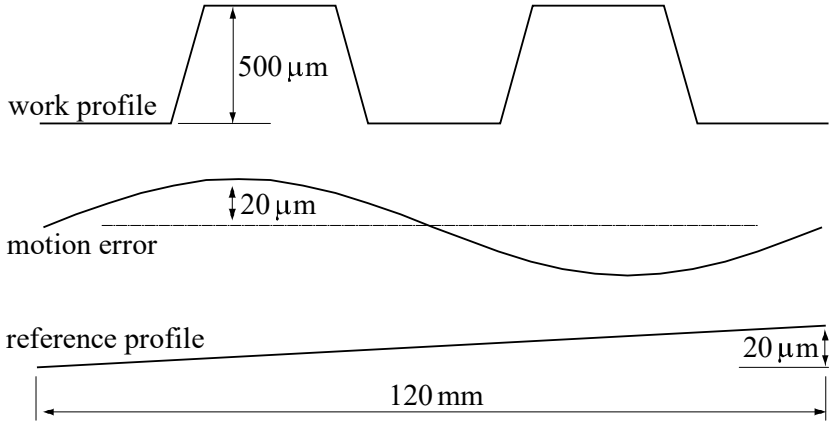

Figure 5. Input signals

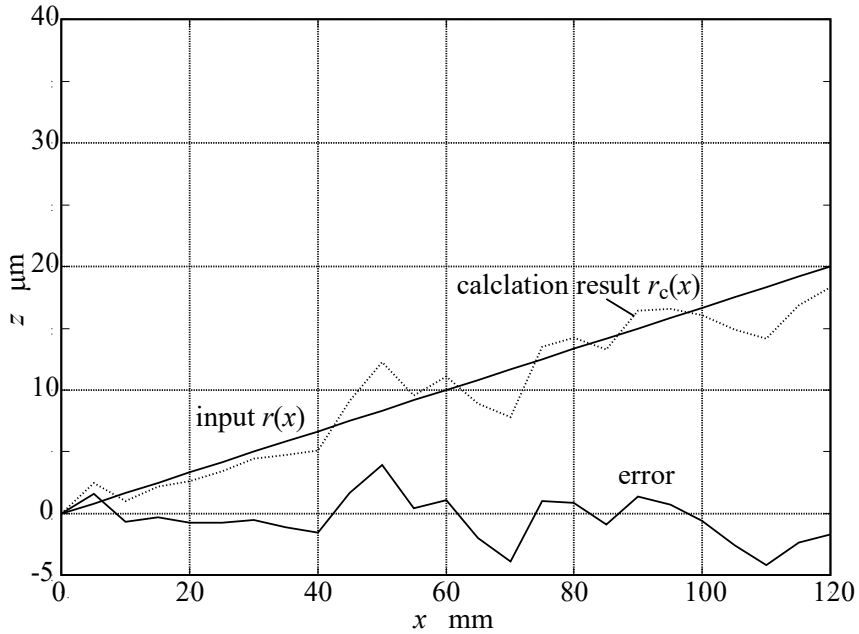

Figure 6. Simulation result of a reference profile measurement

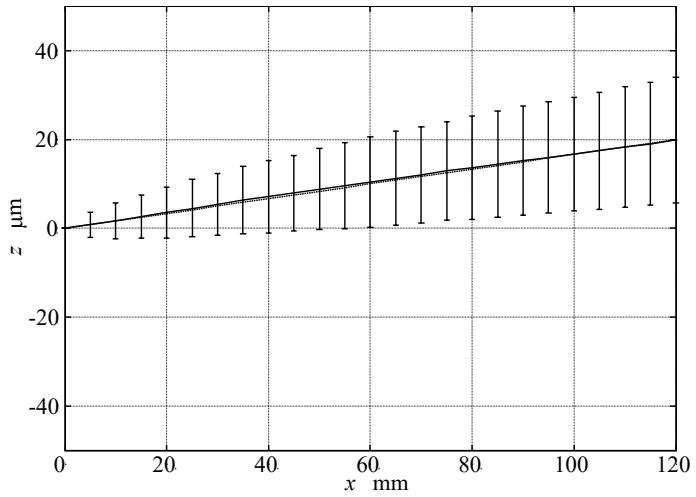

Figure 7. Simulation result of a reference profile measurement and standard deviation calculation

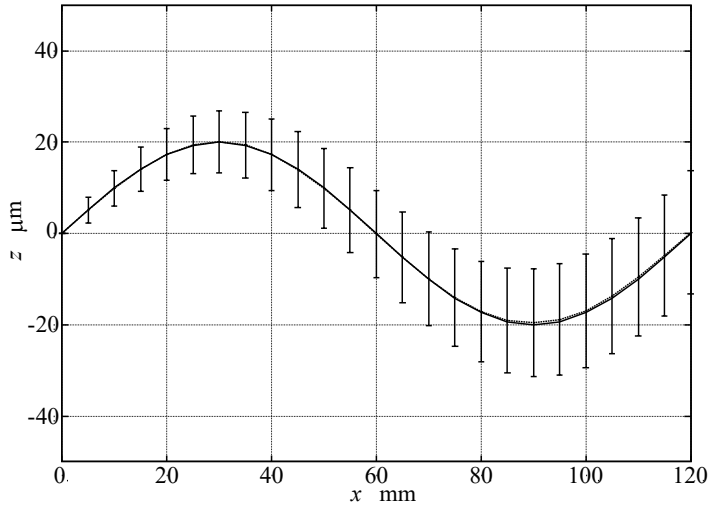

Figure 8. Simulation result of a motion error calculation

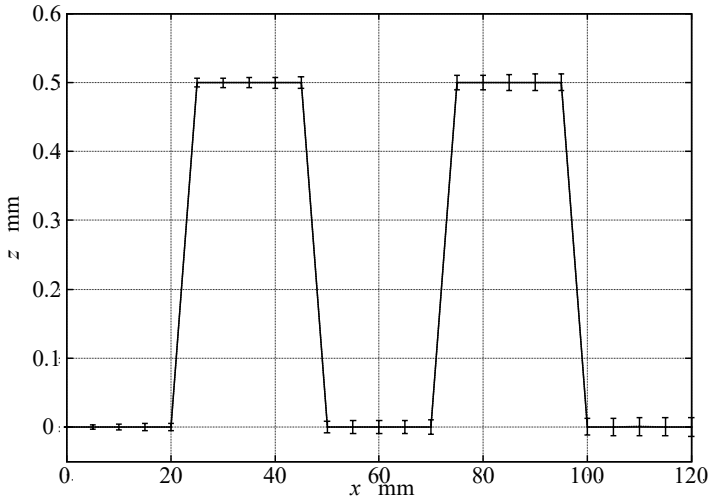

Figure 9. Simulation result of a workpiece profile measurement

The standard deviation is represented by the error bars at each position. The accumulated error affected by the standard deviation increases along the x-axis. Mean values for each position are approximately equal to the input, and it is possible to reduce the effect of random error by averaging. The calculation results of the motion error and workpiece profile are shown in Figure 8 and Figure 9, respectively. Error bars represent the standard deviation for each position. The error of the reference piece profile calculation is affected by the standard deviation of the measuring point. Due to accumulation

error, longer measurement lengths lead to larger standard deviations. The actual measurement results have the potential to occur within the range of these error bars. Therefore, high-accuracy profile measurement is possible with a short measuring length. To confirm the relationship between the error and the measurement length, a simulation was performed by varying the error of the standard deviations.

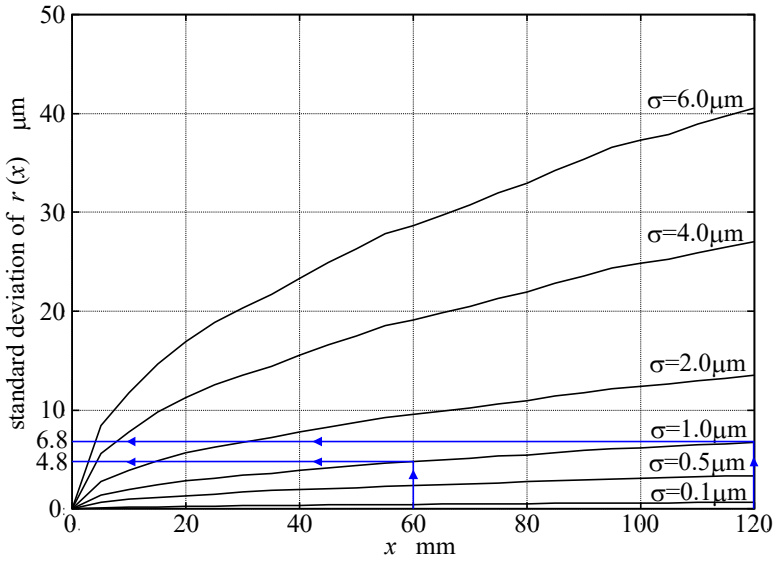

Figure 10. Simulation result of the standard deviation of a reference profile measurement

Figure 10 shows the result of these simulations. The horizontal axis represents the measured position, and the vertical axis represents the standard deviation of $w(x)$ at the measurement position. Moreover, the standard deviation σ of the error for $\delta(x)$ is 0.1 to 6 μm in the simulation. When the measurement error of the reference piece profile is less than a few micrometers (μm), the standard deviation, σ of the measurement error of the reference piece requires less than approximately 1.0 μm at a measurement length of 120 mm. In the case where the measurement length is 60 mm, the error contained in the reference profile $r(x)$ becomes approximately less than 5 μm at each measuring position, and the profile of the reference piece can be measured within an error of 1 μm. If d is reduced, the measurement interval must also be reduced. If d is made infinitely small, the measurement becomes continuous, and a derivative replaces the difference in Eq. (1). However, the sensor's noise must be as low as possible due to the signal-to-noise ratio. Otherwise, the derivative value will be substantial due to noise. This error is contained within $\delta(x_k)$ in Eq. (28), but if the signal-to-noise ratio is poor, the error term will be large even if the positioning error in d is small. Therefore, noise reduction methods such as averaging during measurement are required.

2.3.2 Experimental setup

The prototype experimental apparatus is shown in Figure 11. A table used in a machine tool is used in the experiments. An overview of the prototype measurement system is shown in Figure 11(a). The dimensions of the table of the experimental apparatus were approximately 380 mm × 380 mm × 200 mm, and the traverse range was 120 mm × 120 mm. Moreover, the main components were made of aluminium alloy, and dimensions A to E are shown in Figure 11(b). Reference pieces were built in the table side. In addition, a precision manual linear stage was set between the table and reference piece, and each reference piece was traversed by a micrometre. The respective build-up situations are illustrated in Figure 11(c). The reference piece (X) is set beside the translation table (X), and sensor 1 and sensor 2 are set up on the base plate to measure the reference piece (X). The reference piece (Y) is also set beside the translation table (Y), and sensor 3 and sensor 4 setup on the translation table (Y) are measured by the reference piece (Y). The translation table (Y) on the translation table (X) traverses along the y-axis, and the x-axis and y-axis are orthogonal. Jigs for the sensor No. 1 and No. 2 were made of aluminium alloy (JIS A5052), and each height was 65 mm. Further, Jigs for sensors No. 3 and No. 4 were made of aluminium alloy (JIS A5052), and each height was 70 mm. The dimensions of l_{xs} and l_{xw} in Eq. (24) were 30 mm and 165 mm, respectively. Moreover, the dimensions of l_{ys} and l_{yw} in Eq. (26) were also 30 mm and 165 mm, respectively. A column for sensor No. 0 was made of carbon steel, and the height was 360 mm. The dimensions of the workpiece were 230 mm × 230 mm (t=10 mm), and the dimensions of each reference piece were 380 mm × 60 mm (t =10 mm). Stepper motors (SSA-PE-56D3H, Shinano Kenshi) controlled by Linux CNC drove the table, and the profile of the reference pieces was measured using an eddy current displacement sensor (ML-06, Applied Electronics Corp.). A contact-type displacement sensor (80SB, Tokyo Seimitsu) measured the workpiece profile.

The material of the workpiece and reference pieces were made of carbon steel (JIS S50C). In addition, the workpiece was finished by milling, and the reference pieces were finished by grinding after milling. These were on the base plate (JIS S50C, t = 15 mm). Eddy-current type sensors are used as displacement sensors to measure reference pieces. The eddy-current sensor averages around the sensor head, so the sensor output is obtained as an average value over a diameter.

The diameter of the eddy-current type sensor's heads is 10 mm. Thus, the traverse distance of the reference piece should be 5 mm, which is half of the sensor head. The distance d travelled by the reference piece is set to be the same as the sampling interval. The measurement conditions were as follows: measurement range is 120 mm × 120 mm, sampling interval is 5 mm, traverse distance of the reference piece is 5 mm.

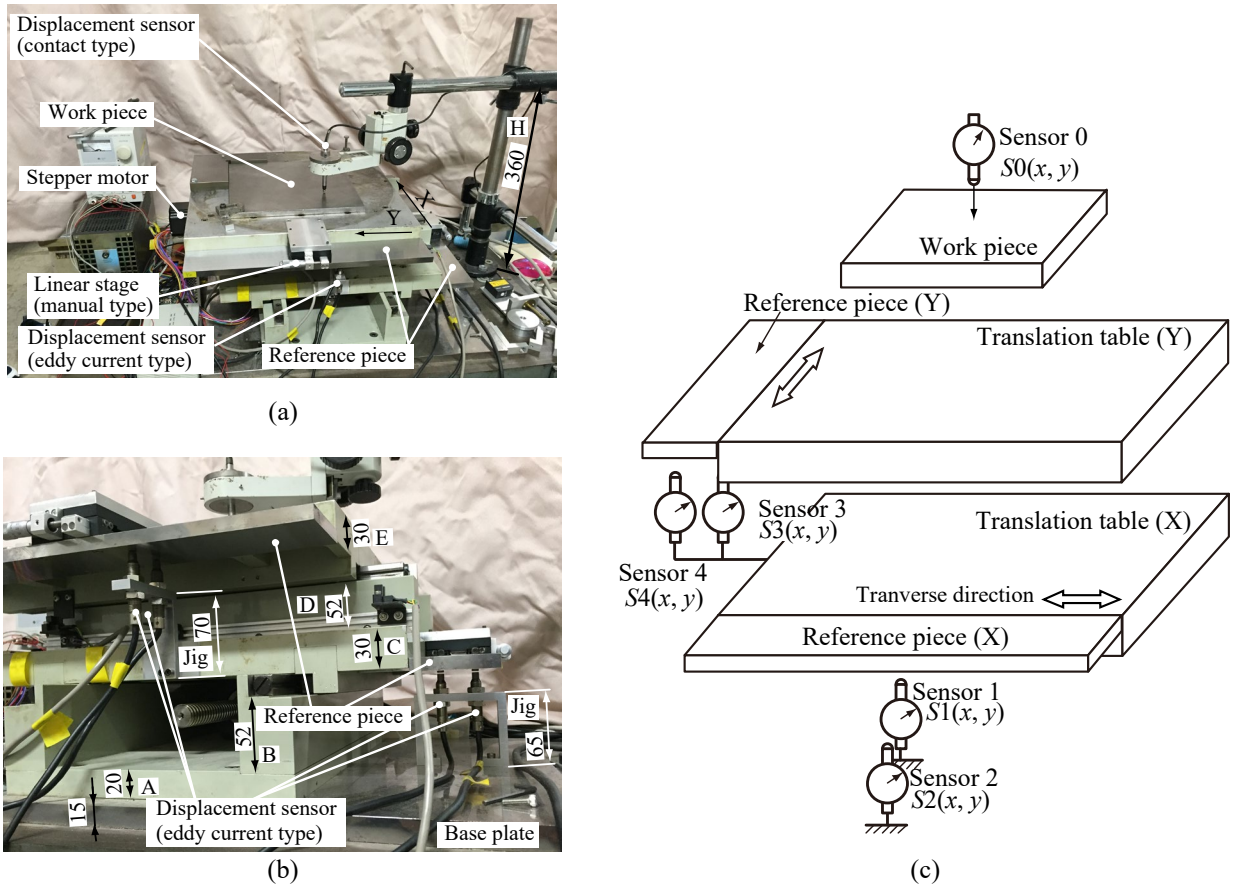

Figure 11. Experimental setup: (a) Overview of the prototype measurement system, (b) Sensors for measuring reference pieces, and (c) Illustration of the setup

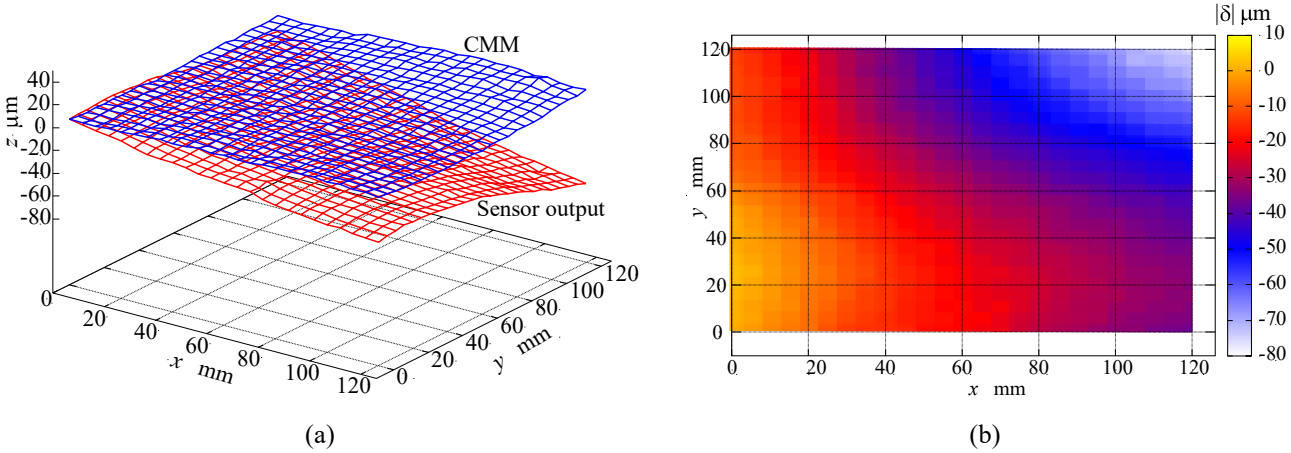

Figure 12. Difference between the proposed method and CMM measurement result: (a) Profile of raw data and CMM measurement results, and (b) Heat map of the difference between the sensor output and CMM results.

2.3.3 Surface profile measurement

In this study, a coordinate measuring machine (CMM) (Crysta-Apex C7106, Mitutoyo) was used to assess the results of the surface profile measurements. Figure 12 shows the results of the surface profile measurements that use a prototype experimental apparatus and CMM for measurement. The result of using the prototype experimental apparatus is raw information. Figure 13 shows the result obtained by removing the motion error using the proposed method and CMM

measurement result. Figures 13(a) and (b) show the surface profile and the difference from CMM by heat map, respectively. The motion error of the traversed table is shown in Figure 12. In particular, the difference from the CMM is larger at positions x = 120 mm and y = 120 mm. The sensor output is −75.8 μm, the CMM measurement result is 6.5 μm, and the difference is approximately 82.3μm at this position. Comparing the results of the proposed method illustrated in Figure 13, the overall shape of the profile with the motion error removed is closer to that of the CMM results. The difference is 9.2 μm at the position of x=120 mm, y=120 mm, and an improvement of 73.1 μm. Let an error be the difference with a CMM measurement result; the sum of squares of the errors is 8130 μm^2 for Figure 12 and 6925 μm^2 in Figure 13, which shows a reduction in error after removing the motion error.

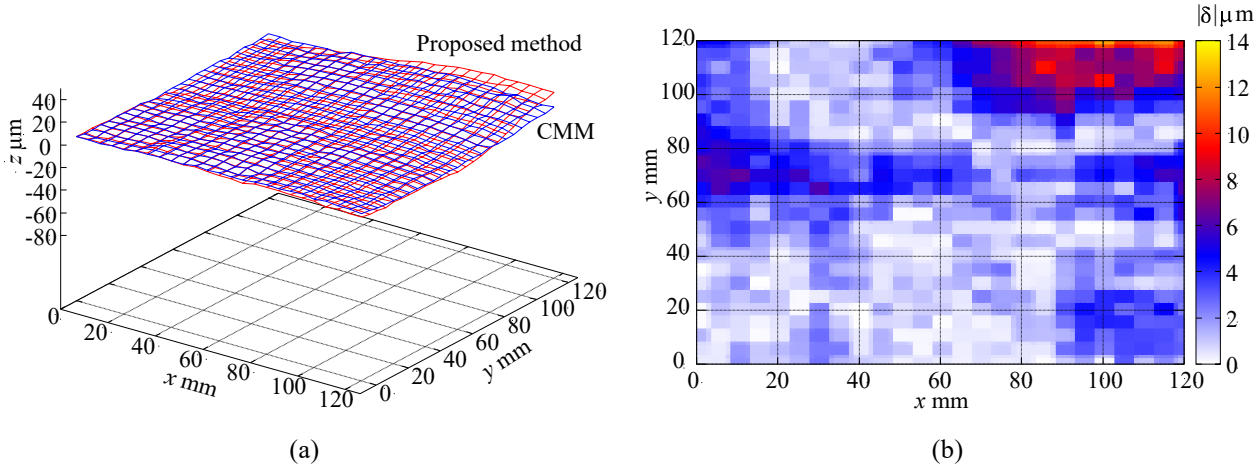

Figure 13. Difference of proposed method and CMM measurement result: (a) Surface profile of the proposed method and CMM measurement result, and (b) Heat map of the difference between the proposed method and the CMM measurement result

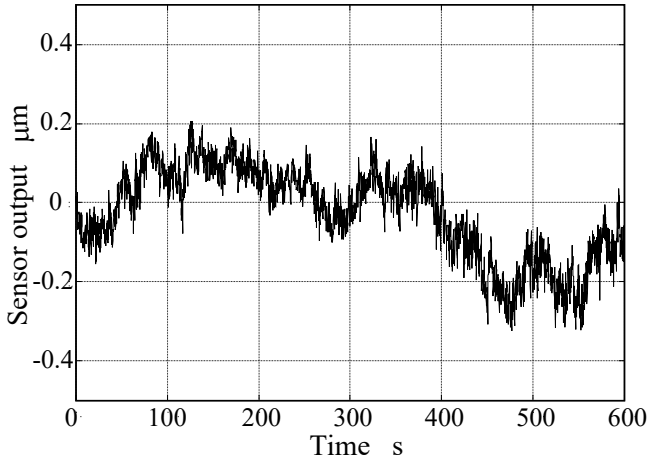

Figure 14. Drift of eddy current type sensor while measuring for 10 min

3. RESULTS AND DISCUSSION

3.1 Sensor Drift

This study performs noise rejection with N = 100, as the sensor error is generally $1/\sqrt{N}$ after N measurements. Figure 14 shows the drift of the eddy current type displacement sensor for 10 min. The sensor output range was −0.3 to 0.2 μm, and the mean was -0.35μm. In addition, the standard deviation was approximately 0.11 μm. Based on the simulation results of Figure 10 and the standard deviation of the eddy current type displacement sensor, the profile of the reference piece can be measured with less than 1μm standard deviation when the measurement range is 120 mm. Therefore, the motion error represented by $m_w(x, y)$ in Eq. (10) includes less than 1.0 μm standard deviation at this measurement length in the reference piece measurement component from Eq. (11) to Eq. (14). Figure 15 shows the drift of the contact-type displacement sensor. The sensor output range is −0.5 to 1.5 μm, and the standard deviation is 0.27 μm. The shape of the workpiece profile represented by $w(x, y)$ in Eq. (10) after the motion error $m_w(x, y)$ was obtained, and even if the error contained in the reference piece measurement was added, the workpiece profile was still measured to be less than 1.5 μm with the standard deviation 0.27 μm at 120 mm measurement length. The results of five measurements

of sensor drift showed that the standard deviation of each sensor output was σ_{se}=0.16 μm for the eddy current type sensor and σ_{sc} = 0.29 μm in contact type sensor.

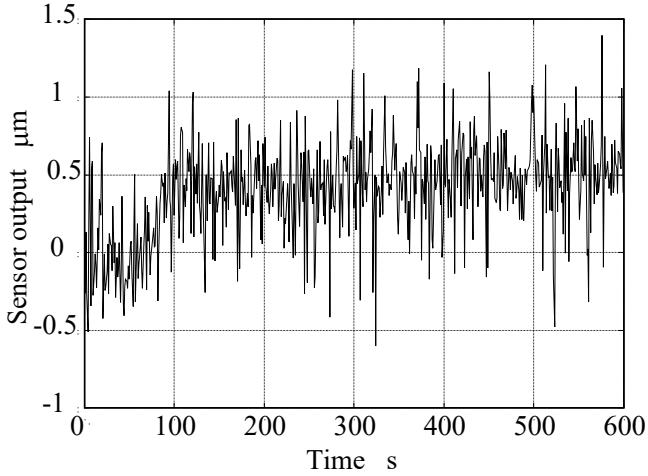

Figure 15. Drift of contact type sensor while measuring for 10 min

3.2 Errors in the Reference Piece Measurement

Figures 16 and 17 show the results of reference piece measurements, respectively. Figure 16 illustrates the measurement results of the reference piece on the x-axis, and Figure 17 illustrates the measurement results on the y-axis. Each figure contains the results of the sensor output (raw data), CMM measurement, and the standard deviation of the measurement result by applying the displacement method. Figure 16 shows that the displacement method is closer to the CMM measurement than the sensor output. The difference between the sensor output and the CMM measurement is 1.35 μm on average, and the difference in maximum is 5.73 μm at x = 85 mm. The difference between the displacement method and the CMM measurement is 1.1 μm with a maximum of 3.01 μm. The standard deviation of the measurement is large at x=120 mm, but the maximum standard deviation is approximately 1μm. These results indicate that the displacement method removes the motion error on the x−axis.

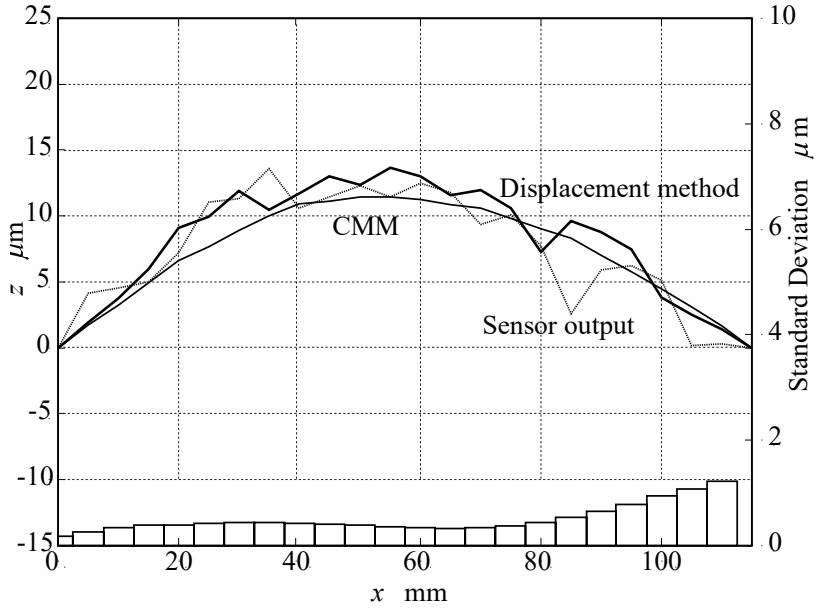

Figure 16. Profile of reference piece set up in x−axis

From Figure 17, the displacement method is closer to the measurement of the CMM than the sensor output. The difference between the sensor output and CMM is 3.54 μm on average and 9.50 μm in maximum, respectively, and the difference between the displacement method and CMM is 2.16 μm on average and 7.71 μm in maximum. These results indicate that the displacement method can remove motion errors on the y-axis as well. The standard deviation of the measurement is larger than that of the x−axis, but the maximum of the standard deviation is less than 4 μm. For the reference piece measurements, the profile of the x-axis reference had a mean, standard deviation of σ_{rx}=0.28 μm. While the profile of the y-axis reference had a mean, standard deviation of σ_{ry}=2.82 μm.

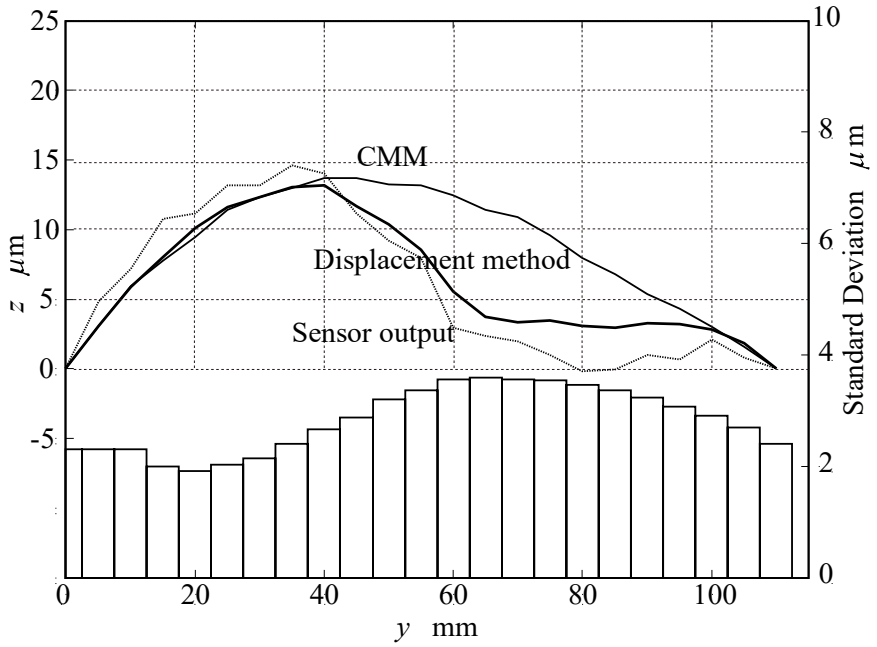

Figure 17. Profile of reference piece set up in y-axis

3.3 Motion Error in Each Axis

This section considers the error components in Eq. (27) and Figure 13. Each term in Eq. (27) is the motion error and the effect of table rotation, and we discuss the motion error. $m2_x\,(x, y)$ and $m4_y\,(x, y)$ are observed by the displacement method using the outputs of sensors No. 2 and No. 4. Figure 18 shows the motion error $m2_x\,(x, y)$ in the x-axis direction, and Figure 19 shows the motion error $m4_y\,(x, y)$ in the y-axis direction. Figure 18(a) shows that the motion error increases in the negative direction as the table travels in the x-axis. By comparing Figure 18 with Figure 12, the sinking of the table in the x−direction, which is not observed in the CMM, is calculated as the motion error $m2_x\,(x, y)$. Hence, the motion error component in the x-axis is appropriately calculated.

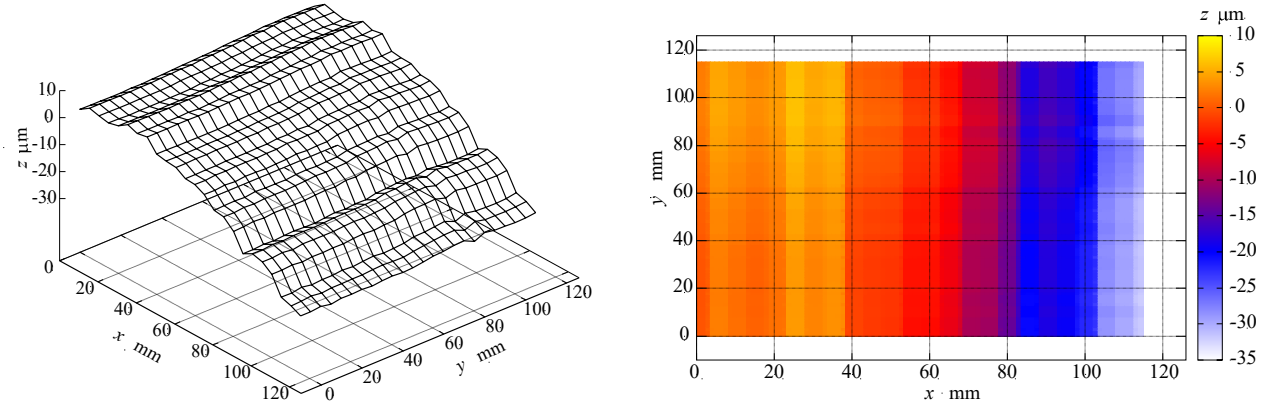

(a) (b)

Figure 18. Motion error about x-axis direction: (a) Profile of motion error in the x-axis direction and (b) Heat map of motion error in the x-axis direction

Similarly, $m4_y\,(x, y)$ increases in the negative direction as the table travels along the y-axis direction in Figure 19. Moreover, $m4_y\,(x, y)$ is maximal at y=120 mm, which indicates that the table sinks along the y-axis direction. By comparing Figure 19 with Figure 12, the motion error component in the y-axis is appropriately calculated as $m4_y\,(x, y)$ in Figure 19 because the z−axis of the sensor output in Figure 12 also increases in the negative direction in the y-axis direction. In N times experiments, the standard deviation $\sigma(x, y)$ can be calculated for each position (x, y). Let the mean of the standard deviation be:

$$\sum_{y}\sum_{x}\sigma(x,y)/XY\,, \tag{29}$$

where, X is the number of measurement positions in the x-axis direction, and Y is the number of measurement positions in the y-axis direction. For the calculation of table motion error, the mean of standard deviation was σ_{m2x}=0.99 μm in the x-axis direction and σ_{m4y}=2.81 μm in the y-axis direction.

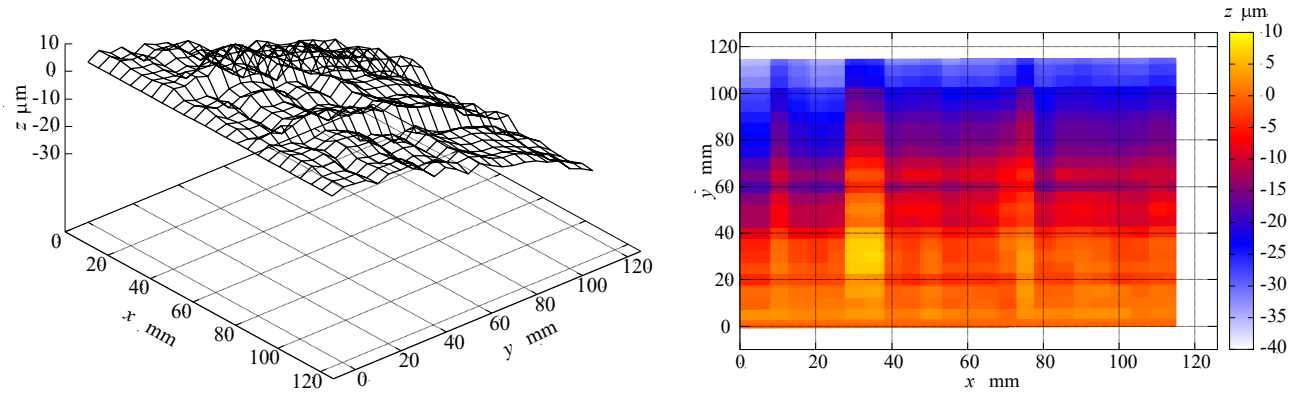

(a) (b)

Figure 19. Motion error about y-axis direction: (a) Profile of motion error in the y-axis direction and (b) Heat map of motion error in the y-axis direction

3.4 Errors Due to the Table Rotation

This section discusses the effect of the errors due to the table rotation. Figure 20 shows the error due to the table rotation in the x-axis direction described as $m_{wxe}(x, y)$ in Eq. (24), and Figure 21 shows the error due to the table rotation in the y-axis direction described as $m_{wye}(x, y)$ in Eq. (26). Both Figures 21(a) show the profiles and (b) show the heat maps. As the table travels, sensors on each of the x and y axes measure the inclination. The motion error just below the sensor for profile measurement was calculated by Eq. (24) and Eq. (26). Figure 20 shows that the error increases along the y-axis direction. This shows that the two sensors (No. 1, No. 2) on the x-axis measure the rotation motion about the x-axis. The maximum error in this case is about 5μm. Similarly, in Figure 21, the error increases along the x-axis direction, and sensors No. 3 and No. 4 measure the error due to table rotation about the y-axis. Here, the error calculated by Eq. (27) is approximately -9 μm at maximum.

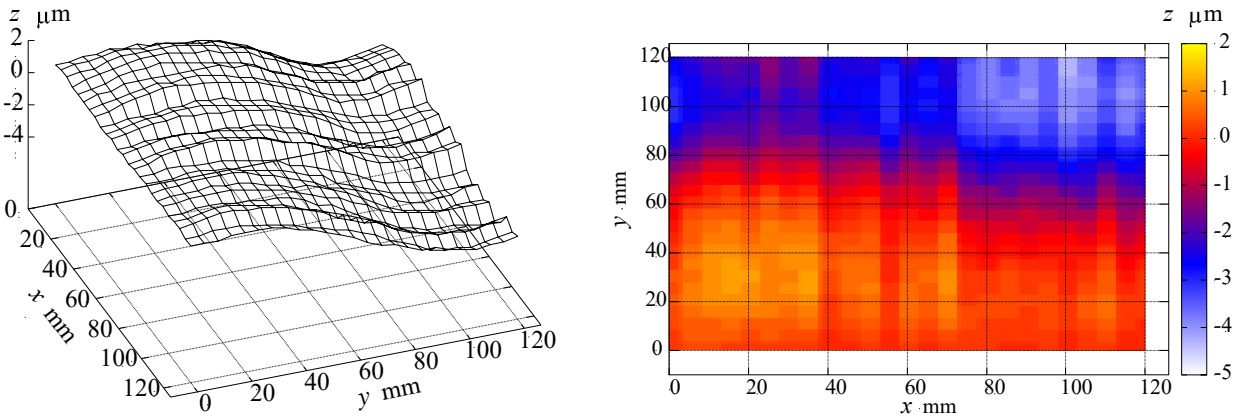

(a) (b)

Figure 20. Effect of table rotation about x-axis direction: (a) Profile of the table rotation effect in the x-axis direction and (b) Heat map of the profile

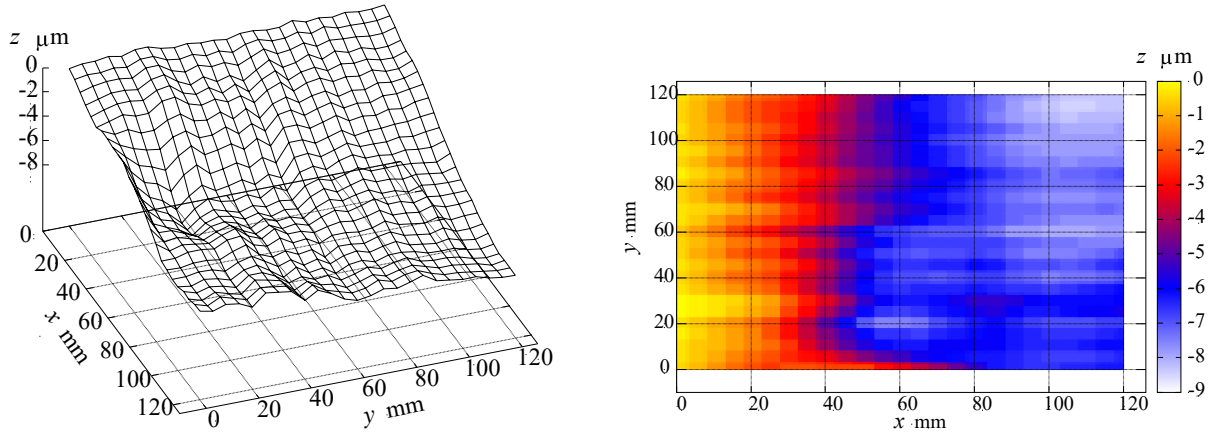

(a) (b)

Figure 21. Effect of table rotation about y-axis direction: (a) Profile of the table rotation effect in the y-axis direction and (b) Heat map of the profile

Figure 22 shows the measurement results without considering the effect of these table rotations, and the difference with the CMM measurement is shown in the heat map. Comparing Figure 22 with Figure 13(b), the error due to table rotation is reduced, especially around y=70 mm. For the error due to the table rotation, the mean of the standard deviation was σ_{mwxe}=1.72 μm and σ_{mwye}=7.43 μm, respectively.

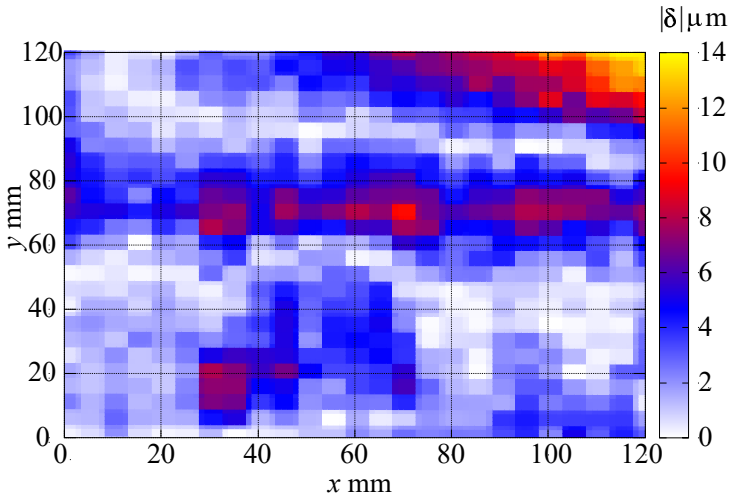

Figure 22. The case of the table position without considering the effect of these table rotations

3.5 Thermal Expansion

The temperature of the measurement environment should not change. A constant-temperature room is highly reliable against temperature changes. This study completed the measurement in a simple airconditioned environment as quickly as possible. In this section, the effect of heat on the measurements is discussed. Thermal effects are very complex and need to be considered for many components [32]. The structure of the prototype experimental apparatus, including the machine structure, lead screws, sensor mounting jigs, bearings, etc., is complex, and it is difficult to study the effects of temperature changes on all of them. Although simulations such as FEM would normally be effective because the parts are fixed with bolts and bearings for guides are built-in, this study was carried out by a simple model assuming that all components are equally affected by temperature changes. Hence, the reference piece, the workpiece, the column, and the components of the translation table are discussed in the following:

The temperature change causes thermal expansion, and the deformation of the material is:

$$\delta_T = \alpha l \Delta T \tag{30}$$

where, α is the coefficient of thermal expansion of the material, l is the dimension of a part, and ΔT is the temperature change. The items in Table 1 are examined for thermal expansion. IT8 was applied to the length of the components of the experimental apparatus. Whereas the column is for the positioning of sensor No. 0, and the tolerance is set to ±1. Further, the coefficient of thermal expansion was determined from the catalogue. First, the temperature changes in the experimental environment are described. As the measurements were carried out in a simple air-conditioned environment, a temperature change of 3-4 ^{0}C was observed in the experiments.

If the uncertainty of the 4 ^{0}C temperature deviation is uniformly distributed, the standard deviation of temperature change becomes:

$$\sigma_t = \frac{2}{\sqrt{3}} = 1.15℃$$

In the following, the thermal expansion with temperature change σ_t is considered. A reference piece for the x-axis is attached to component B. In addition, the measurement jig, components A and B are on the base plate in Figure 11(b). The model for the difference between the reference piece for the x-axis and the sensors No. 1 and No. 2 is:

$$\delta_{Tx} = \left(\alpha_{Al} \cdot l_{dJx} - \alpha_{St} \cdot l_{refx}\right)\Delta T \triangleq \beta_x \Delta T \ , \tag{31}$$

$$l_{dJx} = l_A + l_B - h_{jigx} \ , \tag{32}$$

where α_{Al} and α_{St} are the coefficient of thermal expansion of the aluminum alloy and carbon steel (JIS S50C), respectively.

Moreover, l_A is the thickness of component A, l_B is the thickness of component B, h_{jigx} is the height of the jig for sensor No. 1 (No. 2) and l_{refx} is the thickness of the reference piece. Further, l_{dJx} becomes the difference between the reference piece and the top of the jig.

Table 1. Items to be considered for thermal expansion

Components	Dimensions (mm)	α (μm/m/℃)
Workpiece		
(JIS S50C)	10 ± 0.022	11.7 ± 1.0
Translation table		
A (Aluminium alloy)	20 ± 0.033	23.6 ± 1.0
B (Aluminium alloy)	52 ± 0.046	
C (Aluminium alloy)	30 ± 0.039	
D (Aluminium alloy)	52 ± 0.046	
E (Aluminium alloy)	30 ± 0.039	
Jig for sensor		
x-axis (JIS A5052)	65 ± 0.046	23.6 ± 1.0
y-axis (JIS A5052)	70 ± 0.046	
Reference piece		
(JIS S50C)	10 ± 0.022	11.7 ± 1.0
Base plate		
(JIS S50C)	15 ± 0.027	11.7 ± 1.0
Column		
H (Carbon steel)	360 ± 1	11.7 ± 1.0

Here, the difference between the reference piece for the x-axis and the sensor is obtained,

$$l_{djx} = 20 + 50 - 65 = 7 \text{ mm}$$

, and combined tolerance is,

$$\sigma_{ldJx} = \sqrt{0.033^2 + 0.046^2 + 0.046^2} \simeq 0.074 \text{ mm}.$$

Parts A and B are produced by machining, and jigs are produced by electrical discharge machining, so we thought the products' dimensions would follow a normal distribution. Considering Gauss's error propagation law, variances are obtained as:

$$\sigma_{tx}^2 = \left(\frac{\partial(\delta_{Tx})}{\partial \beta_x}\right)^2 \sigma_{\beta x}^2 + \left(\frac{\partial(\delta_{Tx})}{\partial \Delta T}\right)^2 \sigma_t^2 = (\Delta T)^2 \sigma_{\beta x}^2 + (\beta_x)^2 \sigma_{refx}^2 \tag{33}$$

where, $\sigma_{\beta x}^2$ is a variance of β_x. Similarly, consider Gauss's error propagation law to β_x,

$$\sigma_{\beta x}^2 = \alpha_{Al}^2 \sigma_{ldJx}^2 + l_{dJx}^2 \sigma_{\alpha Al}^2 + l_{refx}^2 \sigma_{\alpha_{st}}^2 + \alpha_{St}^2 \sigma_{lrefx}^2 \tag{34}$$

Here, the uncertainty of the distribution about the coefficient of thermal expansion is a uniform distribution, $\sigma_{\alpha Al}$ and $\sigma_{\alpha St}$ become $(1 \times 10^{-6})/\sqrt{3}$. Hence, each term is obtained as follows:

$$\alpha_{Al}^2 \sigma_{ldx}^2 \ = (23.6 \times 10^{-6})^2 (0.0739 \times 10^{-3})^2 = 3.04167 \ldots \times 10^{-18} \text{ m}^2$$

$$l_{dJx}^2\sigma_{\alpha Al}^2 = (7\times10^{-3})^2\left(10^{-6}/\sqrt{3}\right)^2 = 16.3333\times10^{-18}\ \mathrm{m}^2$$

$$l_{refx}^2\sigma_{\alpha_s t}^2 = (10\times10^{-3})^2\left(10^{-6}/\sqrt{3}\right)^2 = 33.3333\times10^{-18}\ \mathrm{m}^2$$

$$l_{St}^2\sigma_{lrefx}^2 = (11.7\times10^{-6})^2\times(0.022\times10^{-3})^2 = 0.06625\times10^{-18}\ \mathrm{m}^2$$

From the above results,

$$\beta_{\beta x}^2 = 52.7745\ldots\times10^{-18}\ \mathrm{mm}^2$$

whereas,

$$\beta_x = \alpha_{Al}l_{dJx} - \alpha_{St}l_{refx} = 2323.24\times10^{-9}\ \mathrm{m}$$

Substituting ΔT = 4°C into Eq. (33), σ_{tx} is obtained as 0.06 μm.

Similarly, considering error due to thermal expansion for y-axis reference piece measurement. The jig of sensors for measuring the y-axis reference piece is set on the x-axis translation table (component C), and the y-axis translation table is also on the x-axis translation table. Defining the difference between the reference piece and the top of a jig for sensor No. 3 (No. 4) as l_{dJy},

$$l_{dJy} = l_C + l_D - h_{jigy}$$

where, l_C, $l_{D,}$ and h_{jigy} are the thickness of components C, D and the height of the jig for sensor No. 3 (No. 4), respectively. Since l_{dJy} is affected by temperature, the effect of the thermal expansion for the gap of the y-axis measurement is:

$$\delta_{Ty} = \left(\alpha_{Al}l_{dJy} - \alpha_{St}l_{ref\,y}\right)\Delta T \equiv \beta_y\Delta T \tag{35}$$

Considering Gauss's error propagation law, variances are obtained as:

$$\sigma_{ty}^2 = (\Delta T)^2\sigma_{\beta x}^2 + (\beta_x)^2\sigma_{ref\,x}^2 \tag{36}$$

where $\sigma_{\beta y}^2$ is a variance of β_y. Similarly, consider Gauss's error propagation law to β_y,

$$\sigma_{\beta y}^2 = \alpha_{Al}^2\sigma_{ldJy}^2 + l_{ldJy}^2\sigma_{\alpha Al}^2 + l_{ref\,y}^2\sigma_{\alpha_s t}^2 + \alpha_{St}^2\sigma_{lref\,y}^2 \tag{37}$$

A similar calculation as for the x-axis yields σ_{ty} = 0.20 μm. However,

$$l_{djy} = 30\times52 - 70 = 12\ \mathrm{mm}$$

and the combined tolerance,

$$\sigma_{ldjx} = \sqrt{0.046^2 + 0.046^2 + 0.039^2} = 0.076\ \mathrm{mm}$$

is used.

Finally, the effect on sensors for workpiece measurement is discussed. The height from the base plate to the top of the translation table becomes a summation of the thickness of the parts from A to E so that the height becomes 184 mm (h_{tb}). Nevertheless, the base plate and the workpiece are carbon steel, while components A to E are aluminum alloy. A base plate and the workpiece are made of carbon steel (JIS S50C), and each thickness is 15 mm (l_{bp}) and 10 mm (l_{wp}), respectively. Moreover, the column is also made of carbon steel, and its height is 360 mm (h_{col}). Considering the temperature changes affected the difference between the height from the base plate to the workpiece and the height of the column, the model of thermal expansion is

$$\delta_{Tt} = \delta_{bp} + \delta_{tb} + \delta_{wp} - \delta_{col} = \left(\alpha_{St}l_{bp} + \alpha_{Al}h_{tb} + \alpha_{St}l_{wp} - \alpha_S th_{col}\right)\Delta T \equiv \beta_{tt}\Delta T \tag{38}$$

where, δ_{bp}, δ_{tb}, $\delta_{wp,}$ and δ_{col} are the thermal expansions of l_{bp}, h_{tb}, l_{wp} and h_{col}, respectively. Considering Gauss's error propagation law, variances are obtained as:

$$\sigma_{tt}^2 = (\Delta T)^2\,2\sigma_{\beta tt}2 + \beta_{tt}^2\sigma_t^2 \tag{39}$$

where,

$$\sigma_{\beta tt}^2 = \left(l_{bp}^2 + h_{tb}^2 + l_{wp}^2\right)\sigma_{\alpha st}^2 + \left(\sigma_{lbp}^2 + \sigma_{lwp}^2 + \sigma_{hcol}^2\right)\alpha_{St}^2 + h_{tb}^2\sigma_{\alpha Al}^2 + \alpha_{Al}^2\sigma_{thb}^2\ . \tag{40}$$

Thus, we obtained uncertainty of thermal expansion for measurement of the workpiece profile as σ_{tt} = 1.06 μm.

3.6 Consideration of Errors

In the previous section, the errors involved in the proposed method were discussed. In order to obtain the motion error, the reference pieces are measured. Moreover, the measurement error of the reference piece is included in the motion error, so the motion error and the table rotation are the major error sources. The difference between the CMM measurement result and sensor output is 82.3 μm, and the improvement is 73.1 μm at x=120mm, y=120mm. Hence, the motion error accounts for 89% of the errors at x=120 mm y=120 mm. The standard deviation of the eddy current type sensor was σ_{se}

= 0.16μm in the results of five measurements of the sensor drift. If $\delta(x)$ in Equation 28 is considered to appear equally positive and negative, $\sum \delta(x)$ will be a small value. In comparison, the standard deviation of the reference piece is 0.7 μm at x (or y) = 120 mm from Figure 10. Hence, the sensor drift for a motion error of 82.3 μm is considered small. However, owing to the characteristics of the displacement method, if the drift is significant, the cumulative error of the reference piece measurement is large, and consequently, the estimation error of the motion error becomes large.

The rest of the errors are due to table rotation. The difference between the proposed method (without considering table rotation) and the proposed method (with considering table rotation) is 4.6 μm, and the difference between the sensor output and the CMM measurement result is 82.3 μm. Hence, the error accounted for 5.6%. Nevertheless, increasing the number of sensors can also detect the yaw component; thus, a more accurate correction is possible. The correction was too large in the proposed method at x=120 mm and y=120 mm. To improve the accuracy of the correction, it is necessary to increase the accuracy of the motion error estimation. For this purpose, improved methods of reducing the accumulated errors are required. Finally, the uncertainty of the proposed method is discussed. The estimated errors are summarized in Table 2. The dimensions column of Table 1 shows the tolerances for each dimension. The results are as described if the dimensional uncertainties are within this tolerance. IT8 is applied for this tolerance, but IT7 and IT6 would be applied for even more accurate parts. In this case, the variation of the measurement influenced by temperature is smaller, but if the tolerance is larger than IT8, the influence is more significant, and therefore, the uncertainty increases.

Table 2. Estimated errors of the proposed method

Errors	μm	Errors	μm
Sensor drift		**Errors due to the table rotation**	
Eddy current type (σ_{se})	0.16	x-axis (σ_{mwxe})	1.72
Contact type (σ_{sc})	0.29	y-axis (σ_{mwye})	7.43
Reference piece measurement		**Errors due to the thermal expansion**	
x-axis (σ_{sc})	0.28	x-axis (σ_{tx})	0.06
y-axis (σ_{sc})	2.82	y-axis (σ_{ty})	0.20
		translation table (σ_{tt})	1.06
Motion error			
x-axis (σ_{m2x})	0.99		
y-axis (σ_{m4y})	2.81		

Considering thermal expansion, Eq. (10) substituting Eq. (27) can be rewritten as follows:

$$w = m2_x + m4_y - m_{wxe} - m_{wye} - S0 + \theta_{tt} \tag{41}$$

where, (x, y) is omitted, and θ_{tt} is the thermal expansion terms.

Let the variance of w, $m2_x$, $m4_y$, and θ_{tt} be σ_w, σ_{m2x}, σ_{m4y}, σ_{tt}. Further, sensor No. 0 is a contact-type displacement sensor, so that let the variance of $S0$ be σ_{sc}. Moreover, considering Gauss's error propagation law, the variance of w becomes:

$$\sigma_w^2 = \sigma_{m2_x}^2 + \sigma_{m4_y}^2 + \sigma_{mwxe}^2 + \sigma_{mwye}^2 + \sigma_{sc}^2 + \sigma_{tt}^2 = 68.2472\mu m^2$$

Therefore, σ_w becomes 8.26 μm. Other items will also be considered.

$$m2_x = -S2 - r2_x + \theta_{tx} \tag{42}$$

$$m4_y = -S4 - r4_y + \theta_{ty} \tag{43}$$

$$m_{wxe} = \frac{l_{xw}}{l_{xs}}(S1 - S2 + r1_x - r2_x) \tag{44}$$

$$m_{wye} = \frac{l_{yw}}{l_{ys}}(S3 - S4 + r3_y - r4_y) \tag{45}$$

where, θ_{tx} and θ_{ty} are the thermal expansion terms.

Similarly, the sensor No. 1 to No. 4 are the eddy current type displacement sensor, so let the variance of $S1$, $S2$, $S3$, $S4$ be σ_{se}, let the variance of θ_{tx} and θ_{ty} be σ_{tx} and σ_{tx}. Further, assuming the variances of $r1_x$ and $r2_x$ are approximately equal, the variances of $r3_y$ and $r4_y$ are also approximately equal. Let these variances be σ_{rx}, and σ_{ry}, Eq. (42) to Eq. (45) become:

$$\sigma_{m2_x}^2 = \sigma_{se}^2 + \sigma_{rx}^2 + \sigma_{tx}^2 ,$$

$$\sigma_{m4_y}^2 = \sigma_{se}^2 + \sigma_{ry}^2 + \sigma_{ty}^2 ,$$

$$\sigma_{mwxe}^2 = \frac{l_{xw}}{l_{xs}}(\sigma_{se}^2 + \sigma_{se}^2 + \sigma_{rx}^2 + \sigma_{rx}^2)\,,$$

$$\sigma_{mwye}^2 = \frac{l_{yw}}{l_{ys}}\left(\sigma_{se}^2 + \sigma_{se}^2 + \sigma_{ry}^2 + \sigma_{ry}^2\right). \quad (46)$$

Hence, σ_{m2x} = 0.57 μm, σ_{m4y} = 3.00 μm, σ_{mwxe} = 1.07 μm and σ_{mwye} = 9.37 μm are obtained. For σ_{m2x} and σ_{mwxe}, the calculated values are smaller than the measured values. Further, for σ_{m4y} and σ_{mwye}, the calculated values are larger than the measured values. All of them are related to the *y*-axis reference piece, and other error factors are considered to be included in the *y*-axis measurement. Measurement of the *y*-axis reference piece contains errors that cannot be modeled. The experimental apparatus is made of an aluminum alloy, and changing this material changes the thermal expansion. If the material has a smaller thermal expansion, the final uncertainty is smaller, according to Eqs. (30) and (38). In addition, as the error analysis revealed that the errors due to the motion of the *y*-axis and the table rotation are large, the overall measurement accuracy can be increased by increasing the component accuracy for the *y*-axis of the prototype device.

The remaining errors are errors due to positioning accuracy and sensor mounting errors. The positioning error of the translation table depends on the rotational and positioning accuracy of the drive motor due to the machining error of the ball screw. These errors need to be measured separately, which is currently difficult because measuring them in a constant-temperature room is desirable. The deflection of the ball screw is assumed to be so small that it can be ignored in table design. Regarding sensor mounting errors, eddy-current type, and contact type sensors were used in this study, and Abbe's principle is satisfied concerning mounting. In addition, as calibration is carried out before measuring, the installation error was assumed to be negligibly small concerning the installation error. The limitation of the proposed method is when the cumulative error exceeds the permissible value at the desired measurement distance. Therefore, the longer the measurement distance, the greater the uncertainty. A possible solution is to split long measurement distances and subsequently combine the split regions, but the boundary conditions and optimization of the combination require further research.

4. CONCLUSIONS

The displacement method is simple to remove motion errors during on-machine measurements. This study discusses the theory for extending the displacement method to two axes. The extended displacement method measures the reference pieces and the sample simultaneously. The motion error is then detected by measuring the reference piece, and an accurate profile can be measured by subtracting the motion error from the target sample's profile. However, although the displacement method can remove motion errors using a simple principle, it introduces a cumulative error. Therefore, a simulation was conducted to determine how much this cumulative error affects the measurement of the reference piece. Simulations show the limits of the cumulative error. Simulations also show that the cumulative error increases with increasing measurement distance. The results showed that when the sample size is 120 mm, the reference piece can be measured with a cumulative error of less than 7 μm when the measurement error is 1 μm. Conversely, if the cumulative error is to be kept to around 1 μm, the measurement error of the reference strip should be around 0.1 μm. When the measurement interval *d* is reduced, the cumulative error is expected to be even larger because the number of measurement points increases. In this case, the proposed method should be applied by dividing the distance that has to be measured, and a mosaic process is required to join the divided measurement results together, which is a future task.

The position of the stage was modeled and introduced into the theory to reduce tilting errors. Profile measurement experiments were carried out to confirm the problems with improving on-machine measurement in which the motion error of the table traverse is included in the surface profile measurement of the workpiece. Applying the displacement method resulted in an improvement of approximately 88.9%. The error budget was also discussed. The sensor drift was less than the accumulated error of the simulation. The analyzed errors were sensor drift, reference piece measurement errors, motion errors in each axis, and table rotation and thermal expansion errors. From the error budget, it was found that the *y*-axis of the prototype moving table was less accurate than the x-axis. Sensor noise always occurs in reference piece measurements. Future work includes the introduction of machine learning, such as Bayesian linear regression, to model and predict the reference piece to further improve the accuracy, and the system should be more robust.

ACKNOWLEDGMENT

The authors thank the University of Yamanashi, Japan, for their research facilities and support. This study was not supported by grants from funding bodies in the public, private, or not-for-profit sectors.

AUTHOR CONTRIBUTIONS

Y. Haramiishi (Conceptualization; Data curation; Data analysis; Writing - original draft, Writing – review and editing)

Y. A. Rahim (Conceptualization; Data curation; Writing – review and editing)

T. Shimizu (Conceptualization; Supervision; Experimental framework; Data curation; Data analysis; Writing - original draft; Writing – review and editing)

T. Ishii (Writing – review and editing)

M. F. Ali Ahmad (Writing – review and editing)
H. Watanabe (Data analysis; Writing – review and editing)

AVAILABILITY OF DATA AND MATERIALS

The data supporting this study's findings are available on request from the corresponding author.

ETHICS STATEMENT

Not applicable

CONFLICTS OF INTEREST

The authors declare that they have no conflicts of interest to report regarding the present study.

REFERENCES

[1] X. Chen, C. Sun, L. Fu, C. Liu, "A novel reconstruction method for on machine measurement of parallel profiles with a four-probe scanning system," *Precision Engineering*, vol. 59, pp. 224–233, 2019.
[2] T. Tiainen, R. Viitala, T. P. Holopainen, B. Hemming, "Analysis of total rotor runout components with multi-probe roundness measurement method," *Measurement*, vol. 179, p. 109422, 2021.
[3] W. Gao, S. Kiyono, T. Nomura, "A new multiprobe method of roundness measurements," *Precision Engineering*, vol. 19, no. 1, pp. 37–45, 1996.
[4] W. Gao, S. Kiyono, "On-machine roundness measurement of cylindrical workpieces by the combined three-point method," *Measurement*, vol. 21, no. 4, pp. 147–156, 1997.
[5] D. Leete, "Automatic compensation of alignment errors in machine tools," *International Journal of Machine Tool Design and Research*, vol. 1, no. 4, pp. 293–324, 1961.
[6] Y. Zi-qiang, L. Sheng-yi, "Exact straightness reconstruction for on machine measuring precision workpiece," *Precision Engineering*, vol. 29, no. 4, pp. 456–466, 2005.
[7] E. H. Fung, S. Yang, "An approach to on-machine motion error measurement of a linear slide," *Measurement*, vol. 29, pp. 51–62, 2001.
[8] D. Kono, A. Matsubara, I. Yamaji, T. Fujita, "High-precision machining by measurement and compensation of motion error, " *International Journal of Machine Tools and Manufacture*, vol. 48, no. 10, pp. 1103–1110, 2008.
[9] C. Li, S. Li, J. Yu, "High-resolution error separation technique for in-situ straightness measurement of machine tools and workpieces," *Mechatronics*, vol. 6, no. 3, pp. 337–347, 1996.
[10] Y. Zi-qiang, L. Shen-yi, "High accuracy error separation technique for on-machine measuring straightness," *Precision Engineering*, vol. 30, no. 2, pp. 192–200, 2006.
[11] S. Kiyono, W. Gao, "Profile measurement of machined surface with a new differential method," *Precision Engineering*, vol. 16, no. 3, pp. 212–218, 1994.
[12] J. Hwang, C. H. Park, W. Gao, S. W. Kim, "A three-probe system for measuring the parallelism and straightness of a pair of rails for ultra-precision guideways," *International Journal of Machine Tools and Manufacture*, vol. 47, pp. 1053–1058, 2007.
[13] E. Okuyama, H. Akata, H. Ishikawa, "Multi-probe method for straightness profile measurement based on least uncertainty propagation (2nd report) -Two-point method considering cross axis translational motion pitch motion and sensor's random error," *Precision Engineering*, vol. 34, pp. 683–691, 2010.
[14] E. H. K. Fung, M. Zhu, X. Z. Zhang, W. O. Wong, "A novel Fourier eight-sensor (F8S) method for separating straightness, yawing and rolling motion errors of a linear slide," *Measurement*, vol. 47, pp. 777–788, 2014.
[15] E. G. Thwaite, "A method of obtaining an error-free reference line for the measurement of straightness," *Messtechnik*, vol. 10, pp. 317–318, 1973.
[16] X. Ai, T. Shimizu, M. Obi, "Some methods for profile measurement and an application for on-machine measurement," in *IEEE SMC '99 Conference Proceedings*, vol. 4, pp. 481–485, 1999.
[17] X. Ai, T. Shimizu, M. Obi, "Straightness measurement based on using improved displacement method," *The Japan Society of Mechanical Engineers*, vol. 66, pp. 2010–2015, 2000.
[18] W. Gao, J. Aoki, B. F. Ju, S. Kiyono, "Surface profile measurement of a sinusoidal grid using an atomic force microscope on a diamond turning machine," *Precision Engineering*, vol. 31, no. 3, pp. 304–309, 2007.
[19] M. S. Rahman, T. Saleh, H. S. Lim, S. M. Son, M. Rahman, "Development of an on-machine profile measurement system in ELID grinding for machining aspheric surface with software compensation," *International Journal of Machine Tools and Manufacture,* vol. 48, no. 7-8, pp. 887–895, 2008.

[20] H. S. Kim, K. I. Lee, K. M. Lee, Y. B. Bang, "Fabrication of free-form surfaces using a long-stroke fast tool servo and corrective figuring with on-machine measurement," *International Journal of Machine Tools and Manufacture*, vol. 49, pp. 991–997, 2009.

[21] Y. Zhu, J. Na, W. Pan, Y. Zhi, "Discussions on on-machine measurement of aspheric lens-mold surface," *Optik*, vol. 124, pp. 4406–4411, 2013.

[22] R. Jiang, W. Wang, D. Zhang, Z. Wang, "A practical sampling method for profile measurement of complex blades," *Measurement*, vol. 81, pp. 57–65, 2016.

[23] W. Bo, Y. Shimizu, Y. Watanabe, H. Matsukuma, W. Gao, "On machine profile measurement of a micro cutting edge by using a contact-type compact probe unit," *Precision Engineering*, vol. 65, pp. 230–239, 2020.

[24] T. Pfeifer, M. Benz, B. Engelmann, P. Hafner, "High precision ultrasonic on-machine measurement," *Measurement*, vol. 39, pp. 407– 414, 2006.

[25] D. Wang, X. Fu, P. Xu, X. Tian, O. Spires, J. Liang, H. Wu, R. Liang, "Compact snapshot dual-mode interferometric system for on-machine measurement," *Optics and Lasers in Engineering*, vol. 132, p. 106129, 2020.

[26] D. Ding, Z. Zhao, X. Zhang, Y. Fu, J. Xu, "Evaluation and compensation of laser-based on-machine measurement for inclined and curved profiles," *Measurement*, vol. 151, p. 107236, 2020.

[27] O. Borisov, S. Fletcher, A. Longstaff, A. Myers, "Performance evaluation of a new taut wire system for straightness measurement of machine tools," *Precision Engineering*, vol. 38, no. 3, pp. 492–498, 2014.

[28] K. Fan, M. Chen, W. Huang, "A six-degree-of-freedom measurement system for the motion accuracy of a linear stage," *International Journal of Machine Tools and Manufacture*, vol. 38, no. 3, pp. 155–164, 1998.

[29] K. Fan, Y. Zhao, "A laser straightness measurement system using optical fiber and modulation techniques," *International Journal of Machine Tools and Manufacture*, vol. 40, no. 14, pp. 2073–2081, 2000.

[30] N. Huang, Q. Bi, Y. Wang, C. Sun, "5-axis adaptive flank milling of flexible thin-walled parts based on the on-machine measurement," *International Journal of Machine Tools and Manufacture*, vol. 84, pp. 1–8, 2014.

[31] Z. Jiang, B. Song, X. Zhou, X. Tang, S. Zheng, "On-machine measurement of location errors on five-axis machine tools by machining tests and a laser displacement sensor," *International Journal of Machine Tools and Manufacture,* vol. 95, pp. 1–12, 2015.

[32] A. H. Slocum, "Precision machine design," *Society of Manufacturing Engineers*, pp. 96–103, 1992.

[33] A. Breitzke, W. Hintze, "Workshop-suited geometric errors identification of three-axis machine tools using on-machine measurement for long-term precision assurance," *Precision Engineering*, vol. 75, pp. 235–247, 2022

[34] T. Xing, X. Zhao, L. Song, Z. Cui, X. Zou, T. Sun, "On-machine measurement method and geometrical error analysis in a multi-step processing system of an ultra-precision complex spherical surface," *Journal of Manufacturing Processes*, vol. 80, pp. 161–177, 2022.

[35] L. Ye, J. Qian, H. Haitjema, D. Reynaerts, "Uncertainty evaluation of an on-machine chromatic confocal measurement system, " *Measurement*, vol. 216, p. 112995, 2023.